

---

## Single photons from single CdSe quantum dot embedded in ZnSe nanowire

---

T. Aichele<sup>1,+</sup>, G. Sallen<sup>1</sup>, A. Tribu<sup>2</sup>, R. André<sup>1</sup>,  
C. Bougerol<sup>1</sup>, S. Tatarenko<sup>1</sup>, K. Kheng<sup>2</sup> and  
J.-Ph. Poizat<sup>1,\*</sup>

Nanophysics and Semiconductor Group, CEA/CNRS/Université Joseph Fourier,  
(1) Institut Néel, 25 rue des Martyrs,  
38042 Grenoble cedex 9, France

(2) CEA/INAC/SP2M, 38054 Grenoble, France

\*Corresponding author: [jean-philippe.poizat@grenoble.cnrs.fr](mailto:jean-philippe.poizat@grenoble.cnrs.fr)

+ Present address: Physics Institute, Humboldt University, Berlin, Germany

### Abstract:

We report the growth of ZnSe nanowires and nanoneedles using molecular beam epitaxy (MBE). Different growth regimes were found, depending on growth temperature and the Zn–Se flux ratio. By employing a combined MBE growth of nanowires and nanoneedles without any postprocessing of the sample, we achieved an efficient suppression of stacking fault defects. This is confirmed by transmission electron microscopy and by photoluminescence studies. We have inserted a single CdSe quantum dot in these nanowires and we have observed strong photoluminescence from a single CdSe quantum dot embedded in a ZnSe nanowire. Exciton, biexciton and charged exciton lines have been identified unambiguously using photon correlation spectroscopy. This technique has provided a detailed picture of the dynamics of this new system. This type of semi-conducting quantum dot turns out to be a very efficient single photon source in the visible at a temperature as high as 220 K. Its particular growth technique opens new possibilities as compared to the usual self-assembled quantum dots.

**Keywords:** nanowire, quantum dot, optical spectroscopy, single photon, photon correlations

**Biographical notes:** Jean-Philippe Poizat is born in 1965. He got his PhD in 1993 at Institut d'Optique in Orsay under the supervision of Philippe Grangier. He joined the CNRS and continued to work at Institut d'Optique in Orsay in Philippe Grangier's group until 2002. His research topics have been quantum non-demolition measurements, quantum noise of laser diodes and single photon sources from NV centers in diamond. In 2002 he created the "quantum optics" group within the CEA/CNRS/UJF joined team "Nanophysics and semiconductors", of the Laboratoire de Spectrométrie Physique and since 2007 the Néel Institute in Grenoble. His research is on production, manipulation and detection of light at the single photon level. Production and manipulations are performed with semi-conducting quantum dots, and detection with superconducting photodetectors. He has created in 2001 and has been in charge since then of a french network (Groupement de recherche (GdR)) on Quantum information and communication.

**Thomas Aichele** received the Diploma degree in physics from the University of Konstanz, Germany, in 2000 and did his Ph.D. degree work in physics at

University Konstanz and at Humboldt University, Berlin, Germany. From 2005-2007 he has been a Postdoctoral Researcher at Commissariat à l'Énergie Atomique (CEA) and University J. Fourier in Grenoble, France. He is now an assistant professor at Humboldt University, Berlin. His research interests are quantum optics and physics of semiconductor and metal nanostructures.

**Kuntheak Kheng** is Professor at the Grenoble University Joseph Fourier. His interests are the optical properties of quantum dots and quantum wires at the single nanostructure level, the optimization of growth conditions to improve the optical properties, the exploration of possibilities of using nano-emitters for quantum optics. He is the coordinator of the French National Agency (ANR) project BONAFO (2009-2011, <http://pages.ief.u-psud.fr/bonafo/>) whose targets are to get a controlled growth of heterostructures in nanowires, a deep understanding of their optical fundamental properties and evaluate their advantages for opto-electronic applications.

## 1 Introduction

Semiconductor nanowires (NWs) appear as promising building blocks for nanoscale devices and circuits with impressive potential applications including nanoelectronics [1-3], optoelectronics (light emitting diodes [4,5], nanolasers [6]), thermoelectrical energy conversion [7], and biological or chemical sensors [8].

Moreover, high quality defect free nanowires can be grown on low-cost, routinely used substrates such as silicon, which means that they could easily be used for fabricating commercial devices and could possibly be integrated with mainstream Si microelectronics devices.

NW growth methods allow for the variation of the chemical composition [9,10] or doping [11] along the longitudinal or radial directions. This enables the fabrication of well controlled 1D nanoscale heterostructures [10]. For example, as shown in this work, it is possible to insert a slice of a low band gap semiconductor within a high bandgap NW and thus realize a light emitting quantum dot (QD) [12-14]. So far, work on the light emitting properties of single quantum dots has mainly concerned self-assembled QDs formed by surface forces due to lattice mismatch between different materials. They have been widely used in the past decade as single photon sources [15] and for their potential application in quantum information processing (see for example [16,17]). QDs in NWs appears to be an interesting alternative to self-assembled quantum dots. The absence of a wetting layer offers a better confinement which could enable room temperature operation [13]. Radial growth techniques enable engineering of optical guides allowing more efficient light extraction than in bulk materials [18,19]. Furthermore, NW based heterostructures, being much less limited by lattice mismatches, greatly widen the possible material combinations and enable well controlled stacking of several QDs in a single NW, offering interesting possibilities for quantum information processing [20].

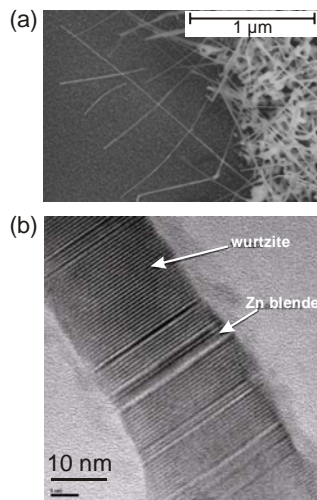
## 2 Nanowire growth and structural properties

Recently, II-VI compound semiconductor NWs have been synthesized by Au-catalysed metal-organic chemical vapour deposition (MOCVD) and molecular-beam epitaxy (MBE) methods [21,22]. An obstacle towards the growth of optically active NW heterostructures are donor-acceptor pairs that form in defects [23]. These cause a strong spectral background which competes with the excitonic emission in the QDs. Reference [24] reports the efficient reduction of this spectral background after annealing of the NW samples in Zn-rich atmosphere.

When developing NW heterostructures, annealing or other postgrowth processing of the sample is often unfavourable as it may also influence the designed form of the heterostructure through interdiffusion of the constituents. Instead, growth methods that directly avoid the formation of defects are desired. We report a growth recipe for ZnSe NWs, where the amount of stacking fault defects is strongly reduced. This was achieved by a combined growth of NWs and nanoneedles without any postgrowth processing of the sample [25].

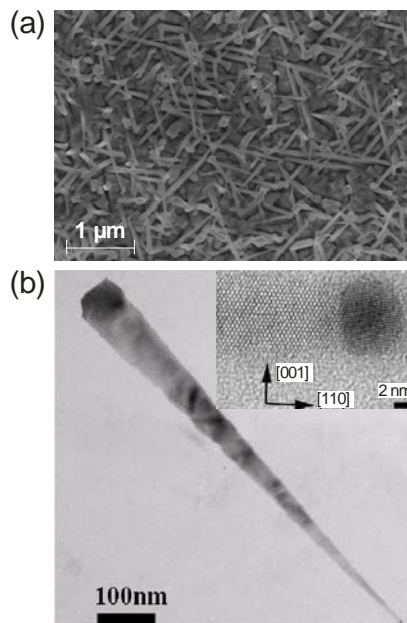
The ZnSe NWs were grown in the vapour-liquid-solid growth mode with gold particles as catalysts. For comparison, GaAs(001) and Si(001) substrates were used. Degassed surfaces for MBE growth were obtained after annealing in ultra-high vacuum at 580° C. In the case of GaAs, the effect of an epitaxial GaAs buffer layer was also investigated. Interestingly the structural properties of the NWs depend very little on the substrate used. Next, a thin gold film with thickness of 0.2 – 0.5 nm was deposited on the GaAs substrates inside an electron beam metal deposition chamber. The gold film was dewetted to a droplet-like surface by annealing the sample at 600° C for 5 min. ZnSe MBE growth was then performed with varying growth conditions. The sample is transferred between the MBE- and metal deposition chambers under ultra-high vacuum.

**Figure 1** Data obtained from NWs grown at 400 °C. (a) SEM image of the as-grown sample at the border of the gold-coated region. The right side shows the dense carpet of NWs. On the left, individual NWs reach into the uncoated zone. (b) TEM image of a single NW. The arrows indicate wurtzite and Zn-blende zones.



When growing under an excess of Se (Zn (Se) flux:  $2.5 (7.5) \times 10^{-7}$  Torr) and a sample temperature of  $350 - 450^\circ \text{C}$ , a dense carpet of narrow NWs with high aspect ratios covers the substrate. The NWs have a uniform diameter of  $20 - 50 \text{ nm}$  and a length up to  $2 \mu\text{m}$  after a growth of one hour (Fig. 1(a)). Additionally to the NWs, the as-grown substrate is covered with highly irregular nano-structures. Fig. 1(b) shows a transmission electron microscopy (TEM) image of one NW. The crystal structure of the NWs are predominantly wurtzite. However, the NWs are systematically intersected with regions of zinc blende phase. We account for the formation of such defects and the presence of highly irregular structures by non-ideal growth conditions at the initial stages of the growth process. Possible reasons are the presence of non-uniform gold agglomerations instead of small gold beads and the insertion of impurities during the gold deposition process. The presence of both wurtzite and Zn-blende shows that, under the growth conditions used, both phases are allowed. Although, the wurtzite structure observed is not the Zn-blende that occurs naturally in bulk ZnSe, it is not an uncommon behaviour for NWs, as discussed in Reference [26].

**Figure 2** Data obtained from nanoneedles grown at  $300^\circ\text{C}$  at Se excess. (a) SEM of the as-grown sample. (b) TEM image of a single nanoneedle. The inset shows a zoom of the region around the tip.

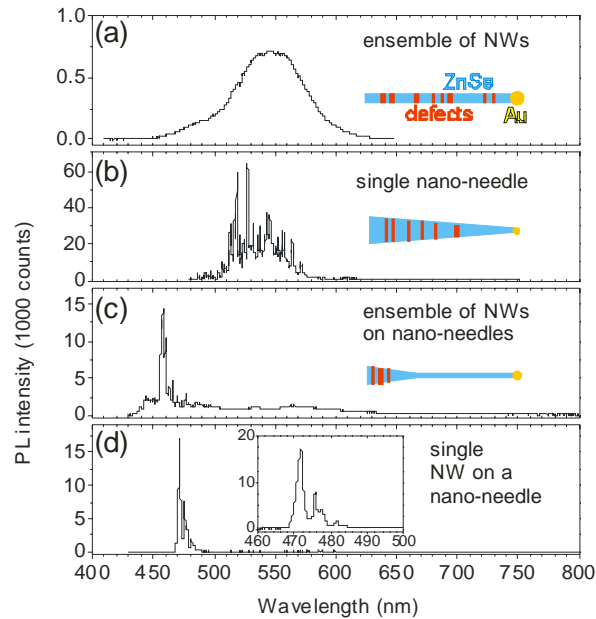


When, on the other hand, growing at low temperature ( $300^\circ \text{C}$ ) or with inverted Zn:Se flux ratio, needle-shaped NWs are formed (fig. 2(a)). Hereafter we will refer to those nanostructures as *nano-needles* to distinguish them from the narrow *NWs* described previously. By TEM (fig. 2(b)) we determined that the nano-needles have a wide base ( $80 \text{ nm}$  in diameter) and a sharp tip ( $5 - 10 \text{ nm}$ ). We also observed darker and lighter regions which again indicate the presence of stacking fault defects. The formation of nano-needles instead of NWs is well accounted for by the slower adatoms mobility expected at low temperature or at low Se flux. The slower mobility promotes nucleation on the

sidewalls before reaching the gold catalyst at the nano-needle tip. Moreover, we observed that the nano-needles are predominantly wurtzite, as for NWs, but the wire axis is here perpendicular to the c-axis instead of being parallel. In contrast also to the long NWs (in Fig. 1), the defect planes are here disoriented with respect to the nano-needle axis. It seems that this disorientation hinders the propagation of defects in the growth direction, especially for lower diameters. Defects zones are rapidly blocked on the side walls, providing a high structural quality towards the nano-needle tip.

To carry out single-NW studies, the sample is put in a methanol ultra-sonic bath for 30 s in order to detach some NWs from the substrate. Droplets of this solution are next placed on a fresh substrate, leaving behind a low density of individual NWs. Ensemble spectra were taken on the as-grown sample. All spectra in this paper were measured at a sample temperature of 5 K. The photoluminescence (PL) of individual NWs were excited with a cw laser at 405 nm via a microscope objective.

**Figure 3** PL spectra from the different samples: (a) NW sample from Fig. 1, (b) nanoneedle sample from Fig. 2, and (c) and (d) combined NW/nanoneedle sample from Fig. 4. The inset of (d) is a zoom into the region of 460–500 nm.

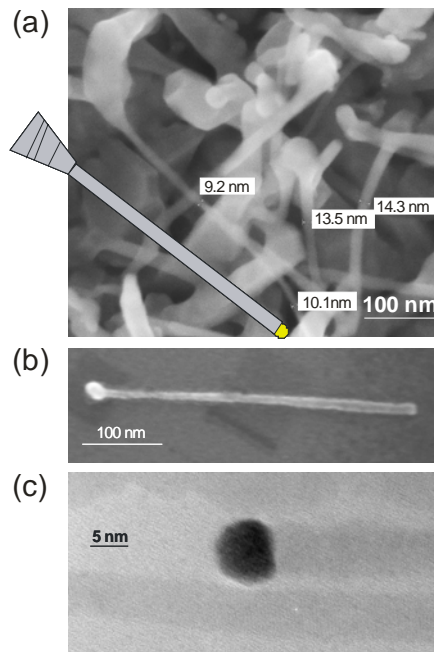


Both for NWs and nano-needles, we observe a broad spectral distribution within 500 – 600 nm, as seen in Figs. 3(a) and (b). Even in the case of a single nano-needle, the spectrum is dominated by many intense spectral lines, which we attribute to emission from excitons localized at the defect zones in the NW [23]. In contrast to the observations in Reference [24] on MOCVD-grown NWs, we do not see an enhancement of the ZnSe band edge emission (443 nm at 5 K [27]) when growing under Zn-rich conditions. The intense emission with 500 – 600 nm instead suggests that in both cases (NWs and nano-needles), point defects effectively capture the excited charge carriers and quench the band

edge emission, as also reported in Reference [28]. This is in agreement with the high density of stacking fault defects observed by TEM.

The observation of a decreasing defect density from the base towards the top in the nano-needles motivated us to modify the growth recipe in the following way: In the first part, the sample is grown with excess of Zn for 30 min, leading to the formation of nano-needle structures. Next, the Zn- and Se-flux was inverted and NWs were grown for another 30 min on top of the nano-needles. Thus, the growth at the side-walls was aborted and re-growth started on defect-free and strain-relaxed nano-needle tips, where the high structural quality of the crystal lattice can be preserved along the narrow NW that is now formed in this second growth step. Fig. 4 shows results obtained from this sample. The structures have a broad base that tapers after a few ten nanometers to thin NWs with thickness of 10 – 15 nm. As symbolized in the sketch in Fig. 4(a) we expect that stacking faults reduce towards the thin part of the NW, which is indeed the case, as seen in TEM images of a single NW, fig. 4(c).

**Figure 4** Data obtained from combined growth of NWs on nanoneedle tips. (a) SEM image of the as-grown NW/nanoneedle sample. (b) SEM of an isolated NW that broke off behind the thicker base. (c) TEM image of two close-by NWs



The suppression of defects has a strong effect on the PL of these nano-structures (Fig. 3). Due to the low density of defects, the spectral emission between 500 – 600 nm that was observed before from the samples in Figs. 3(a) and (b) is strongly reduced, leaving behind only a small bunch of intense spectral lines between 450 – 500 nm. The weak and broad distribution between 500 – 600 nm that remains in the ensemble PL, fig 3(c), is due to excitons localized in defects in the thicker NW base. In the spectrum of a single NW that broke off behind the thicker base, Fig. 3(d), this broad background is now globally

suppressed. In spite of this, no PL is observed at the ZnSe band-edge. A possible reason is that, due to the very thin diameter of the NWs, additional surface states may form in the bandgap [29] and introduce non-radiative decay channels that quench the band-edge PL. The remaining narrow PL peaks around 470 nm in fig. 3(d) can very likely be assigned to residual impurities responsible for donor-acceptor pair emission and their related phonon replica [30].

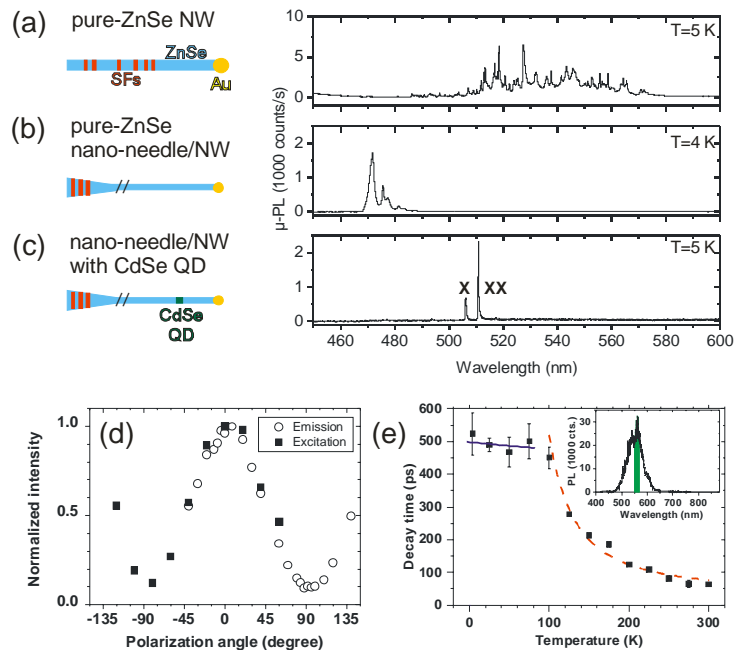
### 3 Optical spectroscopy

For all the optical experiments, samples were mounted on a variable-temperature cryostat allowing experiments from 4 K to room temperature (300 K). The NW emission was efficiently collected by a microscope objective and then dispersed by a monochromator. The sample was either excited by a 405 nm continuous-wave (CW) diode laser or by a 200 fs pulsed frequency-doubled Ti:Sa laser. Panels a-c of Figure 5 compare the PL of single NWs from three different samples at 4-5 K. From a *single*, pure-ZnSe NW grown in a single-step process (Figure 5a), we observe a broad bunch of spectral lines within 500-600 nm, emerging from excitons localized in stacking fault defects along the NW. This is in contrast to NWs grown on top a broader cone-shaped NW base (Figure 5b). As these structures tend to break on the narrower NW part during the ultrasonic bath, a mostly defect-free NW remains. As seen in Figure 5b only few spectral lines remain on these NWs. The displayed ZnSe NW spectrum is one of the most intense found on the sample. Usually, the PL signal is much weaker. We also observe many NWs with practically no PL emission at all on this sample. With these conditions, it finally becomes possible to grow and study single NW samples with an inserted CdSe QD. The PL spectrum of such a NW is depicted in Figure 5c. Similar to single self-assembled QDs, only a few discrete spectral lines remain. A typical  $\mu$ PL spectrum is shown in Fig. 6(a) where three lines can be seen. A comparison with relative energy positions of known emission lines in spectra of self-assembled CdSe/ZnSe QDs [31,32] suggests that these lines correspond to the exciton (X), the biexciton (XX) and the charged exciton (CX). Unambiguous proof for the assignment of these lines will be given below using photon correlation spectroscopy. As we also find many NWs with no PL emission on this sample, the experiments below were performed on preselected NWs, in order to separate them from defective nanostructures that also appear on the substrates. Nevertheless, 1% of the NWs have well-isolated lines enabling single photon generation.

One characteristic feature of such QD NW structures is their polarization behavior. As seen in Figure 5d, the excitation efficiency and the luminescence are both strongly polarization dependent. The PL emission is highly polarized with a contrast of 80-90% (the NW was excited here with a circularly polarized laser light). Conversely, the PL intensity has a sine-like variation as a function of the linear laser polarization. In our case the emitted light is highly polarized with the same direction as the preferred excitation polarization. In previous reports, it was found that the polarization was highly oriented along the NW emission [33,34]. This striking polarization anisotropy of absorption is explained by the dielectric contrast between the NW material and the surrounding environment; the polarization of the emitted light results from a competition between these electromagnetic effects and the orientation of the dipole within the QD [34-36]. Following this argumentation, we think that the polarization is here aligned along the NWs, although we could not verify this alignment, due to limited optical resolution.

Time-resolved measurements of the exciton lifetimes were performed using a streak camera (with a resolution of about 1 ps) on an ensemble of NWs. Figure 5e shows a flat temperature dependence of the decay time at low temperature (below 100 K) followed by an exponential decay above 100 K. The flat temperature dependence is characteristic of three-dimensional confinement (confined excitons) and the exponential decay is characteristic of the nonradiative recombination regime. In the radiative regime, the decay time is about 500 ps and dominates up to 100 K. This is slightly larger than what is observed in self-assembled CdSe/ZnSe QDs (around 300 ps [37]). This could be due to a piezoelectric field resulting from the wurtzite structure in the NWs, which separates electron and hole wave functions and thus reduces the oscillator strength.

**Figure 5** (a-c) PL spectra taken under CW excitation of a single NW structure. The sketches on the left symbolize the shape and composition of each NW (SFs = stacking faults; // = region where the NW is likely to break in the ultrasonic bath): (a) a pure-ZnSe NW grown in a single-step process; (b) a narrow pure-ZnSe NW grown on top of a cone-shaped NW; (c) a narrow ZnSe NW grown on top of a cone-shaped NW and including a CdSe QD zone. (d) Polarization dependence. The solid squares are the variation of the total PL intensity as a function of the polarization of the excitation laser. The open circles are the PL intensity observed through an analyzing polarizer while the excitation laser was circularly polarized. Here, the origin ( $0^\circ$ ) is arbitrarily defined as the angle of maximum intensity. (e) Radiative lifetime of an ensemble of NW structures as a function of the sample temperature. The solid blue (dashed red) curve is a linear (exponential) fit to the data points below (above) 100 K. Inset: Ensemble spectrum that we observed during the time-resolved measurement at 4 K. The green shaded area is the spectral range within which the lifetimes were evaluated.

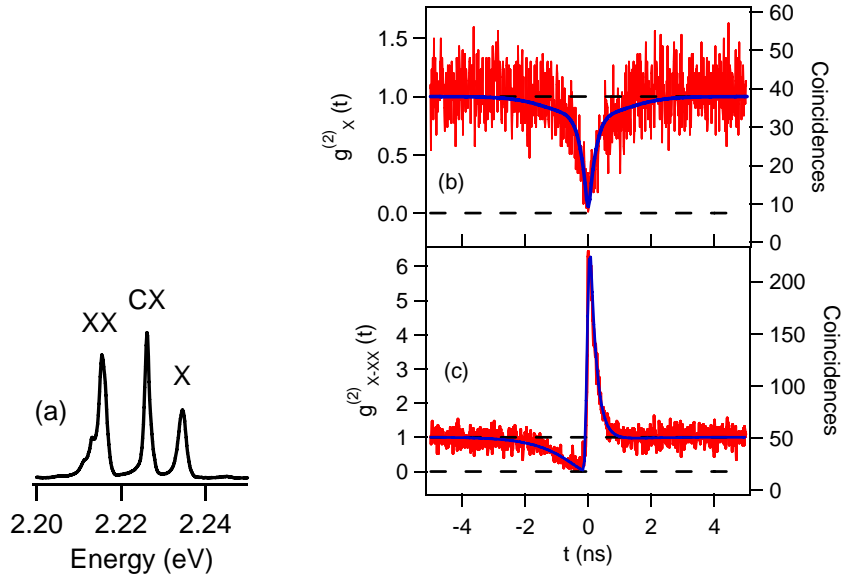


We present now the data for the photon correlation spectroscopy of the neutral QD in fig. 6 [14]. The auto correlation of the X line is shown in Fig. 6(b) exhibiting a clear antibunching which is characteristic of the statistics of a single photon emitter.

Fig. 6(c) shows the cross correlation measurement between the X and the XX line. It displays the typical asymmetric shape with bunching and antibunching features, that is the signature for the cascaded emission of a XX photon followed by a X photon [38,39]. This allows us to identify unambiguously these two lines as exciton and biexciton of the same QD. Note that the narrow bunching peak can only be fitted if the dark exciton is included in the model.

In Fig. 6(b,c), the right vertical axes are the raw number of coincidences. The left axis represent the normalized correlation function according to a Poissonian statistics where the coincidences involving background photons have been subtracted. The corrected correlation function  $g^{(2)}$  is related to the uncorrected one  $g_u^{(2)}$  by  $g^{(2)} - 1 = (g_u^{(2)} - 1)/\rho^2$ , where  $\rho = S/(S+B)$  with S and B respectively the number of signal and background photons as measured in the spectrum of Fig. 6(a) [40].

**Figure 6** (a) displays the spectrum of the QD used for the photon correlation experiments. The lines have been identified as the exciton (X), biexciton (XX) and charged exciton (CX) lines. (b) Exciton autocorrelation, (c) exciton-biexciton cross-correlation. The left axes are the correlation function corrected from the background and the right axes are the raw coincidence rate (see text). The fit is based on a excitonic level scheme including the dark and bright exciton, and the biexciton [14,41]



As can be seen in Fig. 6, the experimental results are very well fitted by an excitonic model including the dark and bright exciton, the biexciton and the charged exciton [14,41] taking into account the temporal resolution of our experimental set-up (90 ps). Inclusion the dark exciton appears essential to the modelling of the photon correlation data. More detailed spectroscopic results on the dark exciton can be found in refs [41,42].

All possible auto-correlation and cross correlations amongst the X, XX, and CX line have also been measured and are well fitted with our model [14,41].

#### 4 Single photon at 220 K

We have carried out photon correlation measurements using a Hanbury Brown and Twiss (HBT) setup with a pulsed laser excitation. For these experiments we used high quantum efficiency APD with lower time resolution than above. Here, the total time resolution of the HBT setup was 850 ps. In order to improve the signal-to-background ratio, we used the strong polarization anisotropy and inserted a linear polarizer oriented for maximum transmission of the spectral line under observation. Under pulsed excitation, the second-order correlation function possesses a peaked structure indicating PL emission on demand. The graphs in Figure 7 are the raw histograms of measured coincidences without any correction for background count events. The area under each peak at  $\tau = 0$ , was normalized with respect to the average area under the peaks at  $|\tau| > 0$ . Each peak area was calculated by integrating the coincidences within 12 ns windows. The correlation functions were taken at different temperatures between 4 and 220 K. At 4 K, the peak at  $\tau = 0$  is suppressed to a normalized value of 7%, showing the high quality of the single-photon generation. With increasing temperature, this value only slightly increases to finally reach 36% at 220 K [13]. This value is far below 50%, the emitted light field is thus clearly distinguished from states with two or more photons. Thus, even without correcting for background events, these emitters can be directly used as a high-quality single-photon device with a strongly suppressed probability for two-photon events, even when operating at high temperature. This was not reported before from a non-blinking semiconductor system [44,45]. Colloidal nanocrystals operate at room temperature but suffer from emission intermittency [46-48].

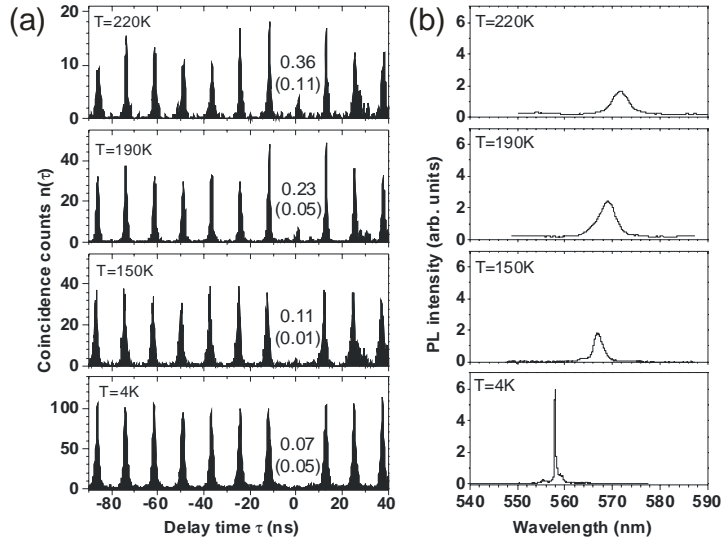
Figure 7b shows the spectra from the NW QD used for the correlation measurements in Figure 7a. With increase in temperature, the spectrum evolves from a dominant trion and a weak exciton transition at 4 K to a broad biexciton line above 150 K. The increased biexciton intensity at high temperature is due to an higher excitation power, which we adjusted at each temperature to achieve an optimized output of the correlation function. Moreover, at high temperature, the biexciton is less affected by nonradiative decay than the exciton due to the shorter biexciton lifetime and due to coupling of bright and dark excitons over spin flips [42,43]. The assignment of the lines to the decay of an exciton, trion, and biexciton was obtained from photon correlation spectroscopy experiments [14].

The analysis of the spectra also allows the contribution of the observed spectral line  $S$  to separate from its spectral background  $B$ . These values can be assessed from integrating the areas under the peak and the spectral background over the corresponding spectral window of the spectrometer output slit. The corrected values are given in Figure 7(a) in parentheses and range within 1%-11%. This shows that the observed spectral lines indeed originate from a single transition.

Although the quality of the single-photon statistics remains mostly constant, the count rate decreases from 25000 counts/s at 4 K to 5000 counts/s at 220 K, and the width of the spectral lines significantly broadens. In the correlation measurements obtained at 190 and 220 K, a low-resolution grating was used in the spectrometer so that all the photons coming from the broader line could be counted. This broader spectral window of integration leads to larger background, which is the main origin for the rise of the  $\tau = 0$

peak above 150 K. In contrast to self-assembled QDs, which often grow with a high density on the substrate, the density of NWs in the microscope focus was much smaller and can be even reduced to only one within the microscope focus (see Figure 4 (b)), which avoids contributions from neighboring emitters that spectrally overlap with the transition under observation. However contributions from other transitions of the same NW cannot be excluded.

**Figure 7** (a) Second-order correlation taken under pulsed excitation at temperatures between 4 and 220 K. The numbers in the graphs are measured values of  $g^{(2)}(0)$  (i.e., the area under the peak at  $\tau = 0$  relative to the peaks at  $|\tau| > 0$ ). The numbers in parentheses are the reconstructed values of the *pure* spectral lines  $g_s^{(2)}(0)$ . (b) Corresponding spectra from the NW QD.



## Conclusions

We have presented a review on a new type of quantum dots inserted in semi-conducting nanowires, namely CdSe QDs embedded in ZnSe NWs. The NWs grown by MBE in a two-step growth recipe, where narrow, mostly defect-free NWs. The high quality of the samples has allowed us to performed optical studies on single CdSe QD inside a ZnSe NW. The single-NW PL is highly polarized with a contrast of 80-90% and features spectral lines from exciton, biexciton, and trion transitions with lifetimes of around 500 ps. When individual transitions were filtered, nonclassical single photon statistics were retrieved, indicated by strong antibunching, where the *raw* correlation function  $g^{(2)}(\tau)$  was reduced down to a normalized value of 7%. This behaviour remains even up to a temperature of 220 K, where this correlation peak is only slightly increased to 36%. For nonblinking QDs, this is the highest reported temperature for

single-photon emission and for an antibunching dip below 50%. At this temperature, Peltier cooling becomes an alternative to liquid helium or nitrogen cooling. Together with the possibility of integrating NWs into electro-optical circuits, these emitters become an interesting candidate for developing compact, stable, and cost-efficient quantum devices operating near room temperature.

## Acknowledgements

We thank L. Besombes and M. Richard for many fruitful discussions, F. Donatini for very efficient technical support. T.A. acknowledges support by Deutscher Akademischer Austauschdienst (DAAD). Part of this work was supported by European project QAP (Contract No. 15848).

## References

- 1 Duan, X., Huang, Y., Cui, Y., Wang, J., and Lieber, C. M. (2001) 'Indium phosphide nanowires as building blocks for nanoscale electronic and optoelectronic devices', *Nature*, Vol. **409**, 66.
- 2 Lu, W., and Lieber, C. M. (2007) 'Nanoelectronics from the bottom up', *Nature Materials*, Vol. **6**, 841.
- 3 Thelander, C., Martensson, T., Björk, M. T., Ohlsson, B. J., Larsson, M. W., Wallenberg, L. R., and Samuelson, L. (2003) 'Single-electron transistors in heterostructure nanowires', *Appl. Phys. Lett.*, Vol. **83**, 2052.
- 4 Könenkamp, R., Word, R. C., Schlegel, C. (2004) 'Vertical nanowire light-emitting diode', *Appl. Phys. Lett.*, Vol. **85**, 6004.
- 5 Kim, H.M., Cho, Y.H., Lee, H., Kim, S.I., Ryu, S.R., Kim, D.Y., Kang, T.W., and Chung, K.S. (2004) 'High-brightness light emitting diodes using dislocation-free indium gallium nitride/gallium nitride multi-quantum-well nanorod arrays', *Nano Lett.*, Vol. **4**, 1059.
- 6 Duan, X., Huang, Y., Agarwal, R. and Lieber, C. M. (2003) 'Single-nanowire electrically driven lasers', *Nature*, Vol. **421**, 241.
- 7 Hochbaum, A.I., Chen, R., Delgado, R.D., Liang, W., Garnett, E.C., Najarian, M., Majumdar, A., and Yang, P. (2008) 'Enhanced thermoelectric performance of rough silicon nanowires', *Nature*, Vol. **451**, 163.
- 8 Cui, Y., Wei, Q., Park, H., and Lieber, C. M. (2001) 'Nanowire nanosensors for highly sensitive and selective detection of biological and chemical species', *Science*, Vol. **293**, 1289.
- 9 Gudiksen, M. S., Lauhon, L., Wang, J., Smith, D. C., and Lieber, C. M. (2002) 'Growth of nanowire superlattice structures for nanoscale photonics and electronics', *Nature*, Vol. **415**, 617.
- 10 Björk, M. T., Ohlsson, B. J., Sass, T., Persson, A. I., Thelander, C., Magnusson, M. H., Deppert, K., Wallenberg, L. R., and Samuelson, L. (2002) 'One-dimensional steeplechase for electrons realized', *Nanolett.* Vol. **2**, 87, *Appl. Phys. Lett.*, Vol. **80**, 1058.
- 11 Yang, C. Zhong, Z., and Lieber, C. M. (2005) 'Encoding electronic properties by synthesis of axial modulation-doped silicon nanowires', *Science*, Vol. **310**, 1304.
- 12 Borgström, M. T., Zwiller, V., Müller, E., and Imamoglu, A. (2005) 'Optically bright quantum dots in single nanowires', *Nano Lett.*, Vol. **5**, 1439.

- 13 Tribu, A. Sallen, G., Aichele, T., André, R., Poizat, J.-Ph. Bougerol, C. Tatarenko, S. And Kheng, K. (2008) 'A High-Temperature Single-Photon Source from Nanowire Quantum Dots', *Nano Lett.*, Vol. **8**, 4326.
- 14 Sallen, G. Tribu, A. Aichele, T., André, R., Bougerol, C., Tatarenko, S., Kheng, K. and Poizat, J.Ph. (2009) 'Photon correlation spectroscopy on a single quantum dot embedded in a nanowire', arXiv:0903.0806v1.
- 15 Michler, P. Kiraz, A. Becher, C. Schoenfeld, W.V. Petroff, P.M. Zhang, L. Hu, E. and Imamoglu, A. (2000) 'A quantum dot single-photon turnstile device', *Science*, Vol. **290**, 2282.
- 16 Fushman, I., Englund, D., Faraon, A., Stoltz, N, Petroff, P., and Vuckovic, J. (2008) 'Controlled phase shifts with a single quantum dot', *Science*, Vol. **320**, 769.
- 17 Hanson, R., and Awschalom, D.D. , (2008) 'Coherent manipulation of single spins in semiconductors' *Nature*, Vol. **453**, 1043.
- 18 Pauzauskie, P.J. Yang, P. , (2006) 'Nanowire photonics', *Materials Today*, Vol. **9**, 36
- 19 Gregersen, N., Nielsen, T.R., Claudon, J., Gérard, J.M., and Mork, J. (2008) 'Controlling the emission profile of a nanowire with a conical taper', *Opt. Lett.*, Vol **33**, 1693.
- 20 Simon, C., Niquet, Y.M., Caillet, X., Eymery, J., Poizat, J.P., Gérard, J.M. (2007) 'Quantum communication with quantum dot spins', *Phys. Rev. B*, Vol. **75**, 081302.
- 21 Solanki, R., Huo, J., Freeouf, J. L., and Miner, B. (2002) 'Atomic layer deposition of ZnSe/CdSe superlattice nanowires', *Appl. Phys. Lett.*, Vol. **81**, 3864.
- 22 Chan, Y. F., Duan, X. F., Chan, S. K., Sou, I. K Zhang, X. X., and Wang, N. (2003) 'ZnSe nanowires epitaxially grown on GaP(111) substrates by molecular-beam epitaxy', *Appl. Phys. Lett.*, Vol. **83**, 2665. Colli, A., Hofmann, S Ferrari, A. C. Ducati, C Martelli, .F Rubini, .S. Cabrini, S. Franciosi, A. and Robertson, J. (2005) 'Low-temperature synthesis of ZnSe nanowires and nanosaws by catalyst-assisted molecular-beam epitaxy', *Appl. Phys. Lett.*, Vol. **86**, 153103.
- 23 Philipose, U., Yang, S., Xu, T., and Ruda, H. E. (2007) 'Origin of the red luminescence band in photoluminescence spectra of ZnSe nanowires', *Appl. Phys. Lett.*, Vol. **90**, 063103.
- 24 Philipose, U., Xu, T., Yang, S., Sun, P., Ruda, H. E., Wang, Y. Q., and Kavanagh, K. L. (2006) 'Enhancement of band edge luminescence in ZnSe nanowires', *J. Appl. Phys.*, Vol **100**, 084316
- 25 Aichele, T. Tribu, A. Bougerol, C. Kheng, K. André, R., Tatarenko, S. (2008) 'Defect-free ZnSe nanowire and nanoneedle nanostructures', *Appl. Phys. Lett.*, Vol. **93**, 143106.
- 26 Glas, F. Harmand, J.-C. and Patriarche, G. (2007) 'Why does wurtzite form in nanowires of III-V zinc blende semiconductors?', *Phys. Rev. Lett.*, Vol. **99**, 146101.
- 27 Malikova, L., Krystek, W., Pollak, F. H., Dai, N., Cavus, A., and Tamargo, M. C. , (1996). 'Temperature dependence of the direct gaps of ZnSe and Zn<sub>0.56</sub>Cd<sub>0.44</sub>Se', *Phys. Rev. B* **54**, 1819.
- 28 Xiang, B., Zhang, H. Z., Li, G. H., Yang, F. H., Su, F. H., Wang, R. M., Xu, J., Lu, G., W. Sun, X. C. Zhao, Q., and Yu, D. P. (2003) 'Green-light-emitting ZnSe nanowires fabricated via vapor phase growth', *Appl. Phys. Lett.*, Vol. **82**, 3330.
- 29 Schmidt, T. M. (2006) 'Hydrogen and oxygen on InP nanowire surfaces', *Appl. Phys. Lett.*, Vol. **89**, 123117.
- 30 Polimeni, A., Capizzi, M., Nabetani, Y. Ito, Y., Okuno, T. Kato, T., Matsumoto, T., and Hirai, T. (2004) 'Temperature dependence and bowing of the bandgap in ZnSe<sub>1-x</sub>O<sub>x</sub>' *Appl. Phys. Lett.*, Vol. **84**, 3304. Weinstein, B., A. Ritter, T. M., Strachan, D., Li, M., Luo, H., Tamargo, M., and Park, R. (1996) 'Competition of deep and shallow impurities in wide-gap II-VI semiconductors under pressure', *Phys. Status Solidi B.*, Vol. **198**, 167.
- 31 Türck, V., Rodt, S., Heitz, R., Stier, O. Strassburg, M. Pohl, U. W., and Bimberg, D. (2001), 'Charged excitons and biexcitons in self-organized CdSe quantum dots', *Phys. Status Solidi b*, Vol. **224**, 217.

- 32 Patton, B., Langbein, W., and Woggon, U. (2003) 'Trion, biexciton, and exciton dynamics in single self-assembled CdSe quantum dots', *Phys. Rev. B*, Vol. **68**, 125316.
- 33 Wang, J., Gudiksen, M. S., Duan, X., Cui, Y., Lieber, C. M. (2001) 'Highly polarized photoluminescence and photodetection from single indium phosphide nanowires', *Science*, Vol. **293**, 145
- 34 Lan, A., Giblin, J., Protasenko, V., and Kuno, M. (2008) 'Excitation and photoluminescence polarization anisotropy of single CdSe nanowires', *Appl. Phys. Lett.*, Vol. **92**, 183110.
- 35 Niquet, Y. M., and Mojica, D. C. (2008) 'Quantum dots and tunnel barriers in InAsOInP nanowire heterostructures: Electronic and optical properties', *Phys. Rev., B*, Vol. **77**, 115316.
- 36 van Weert M. H. M. et al, (2008) 'Polarization Properties of Single Quantum Dots in Nanowires' arXiv:0808.2908.
- 37 Bacher, G., Weigand, R., Seufert, J., Kulakovskii, V. D., Gippius, N. A., and Forchel, A. (1999) 'Biexciton versus exciton lifetime in a single semiconductor quantum dot', *Phys. Rev. Lett.*, Vol. **83**, 4417.
- 38 Moreau, E., Robert, I., Manin, L., Thierry-Mieg, V., Gérard, J. M., Abram, I. (2001) 'Quantum cascade of photons in semiconductor quantum dots', *Phys. Rev. Lett.*, Vol. **87**, 183601.
- 39 Couteau, C., Moehl, S., Tinjod, F., Gérard, J. M., Kheng, K., Mariette, H., Gaj, J. A., Romestain, R., and Poizat, J. Ph. (2004) 'Correlated photon emission from a single II-VI quantum dot' *Appl. Phys. Lett.*, Vol. **85**, 6251.
- 40 Brouri, R., Beveratos, A., Poizat, J.Ph., and Grangier, Ph. (2000) 'Photon antibunching in the fluorescence of individual color centers in diamond', *Opt. Lett.*, Vol. **25**, 1294.
- 41 Sallen, G., (2009) 'Spectroscopie optique de boîtes quantiques de CdSe insérées dans des nanofils de ZnSe', PhD thesis, Université Joseph Fourier, Grenoble <http://tel.archives-ouvertes.fr/tel-00362497/fr/>
- 42 Reischle, M., Beirne, G. J., Rossbach, R., Jetter, M., and Michler, P. (2008) 'Influence of the dark exciton state on the optical and quantum optical properties of single quantum dots', *Phys. Rev. Lett.*, Vol. **101**, 146402
- 43 Sallen, G., Tribu, A., Aichele, T., André, R., Besombes, L., Bougerol, C., Tatarenko, S., Kheng, K. and Poizat, J.Ph. (2009) 'Dark exciton optical spectroscopy of a semiconducting quantum dot embedded in a nanowire', arXiv:0903.0497.
- 44 Sebald, K., Michler, P., Passow, T., Hommel, D., Bacher, G., Forchel, A. (2002) 'Single-photon emission of CdSe quantum dots at temperatures up to 200 K', *Appl. Phys. Lett.*, Vol. **81**, 2920.
- 45 Kako, S., Santori, C., Hoshino, K., Götzinger, S., Yamamoto, Y., and Arakawa, Y. (2006) 'A gallium-nitride single-photon source operating at 200K', *Nat. Mater.*, Vol. **5**, 887.
- 46 Michler, P., Imamoglu, A., Mason, M. D., Carson, P. J., Strouse, G. F., Buratto, S. K. (2000) 'Quantum correlation among photons from a single quantum dot at room temperature', *Nature*, Vol. **406**, 968.
- 47 Brokmann, X., Giacobino, E., Dahan, M., and Hermier, J. P. (2004) 'Highly efficient triggered emission of single photons by colloidal CdSe/ZnS nanocrystals', *Appl. Phys. Lett.*, Vol. **85**, 712.
- 48 Mahler, B., Spinicelli, P., Buil, S., Quelin, X., Hermier, J.P., and Dubertet, B. (2008) 'Towards non-blinking colloidal quantum dots', *Nature Materials*, Vol. **7**, 659.